20. J. Hlavatý, J. Rathousky, A. Zukal, L. Kavan, *Carbon* **39**, 53 (2000).
21. A. Baeyer, *Ber. Dtsch. Chem. Ges.* **18**, 2269 (1885).
22. F. Straus, L. Kollek, H. Hauptmann, *Ber. Dtsch. Chem. Ges. B.* **63B**, 1886 (1930).
23. E. Heilbronner, V. Hornung, J. P. Maier, E. Kloster-Jensen, *J. Am. Chem. Soc.* **96**, 4252 (1974).
24. J. A. Webb, P.-H. Liu, O. L. Malkina, N. S. Goroff, *Angew. Chem. Int. Ed. Engl.* **41**, 3011 (2002).
25. C. Laurence, M. Queignec-Cabanetos, T. Dziembowska, R. Queignec, B. Wojtkowiak, *J. Am. Chem. Soc.* **103**, 2567 (1981).
26. C. Laurence, M. Queignec-Cabanetos, B. Wojtkowiak, *Can. J. Chem.* **61**, 135 (1983).
27. J. A. Webb, J. E. Klijn, P. A. Hill, J. L. Bennett, N. S. Goroff, *J. Org. Chem.* **69**, 660 (2004).
28. P. D. Rege, O. L. Malkina, N. S. Goroff, *J. Am. Chem. Soc.* **124**, 370 (2002).
29. W. N. Moss, N. S. Goroff, *J. Org. Chem.* **70**, 802 (2005).
30. P. Metrangolo, G. Resnati, *Chem. Eur. J.* **7**, 2511 (2001).
31. A. Crihfield *et al.*, *Cryst. Growth Des.* **3**, 313 (2003).
32. N. S. Goroff, S. M. Curtis, J. A. Webb, F. W. Fowler, J. W. Lauher, *Org. Lett.* **7**, 1891 (2005).
33. H. M. Yamamoto, J. I. Yamaura, R. Kato, *Synth. Met.* **102**, 1448 (1999).
34. H. M. Yamamoto, J. I. Yamaura, R. Kato, *Synth. Met.* **102**, 1515 (1999).
35. Materials and methods are available as supporting material on *Science* Online.
36. S. Coe *et al.*, *J. Am. Chem. Soc.* **119**, 86 (1997).
37. T. L. Nguyen, F. W. Fowler, J. W. Lauher, *J. Am. Chem. Soc.* **123**, 11057 (2001).
38. For example, in the **2•6** co-crystal, the iodine-nitrogen halogen bonding distance is 3.07 Å, and the C–I–N angle is 174.4°. In contrast, the iodine-nitrogen distance in the **1•7** co-crystal is 3.21 Å, and the C–I–N angle is 167.8°. The iodine-oxygen close contact is similar, with a distance of 3.20 Å and angle of 168.5°.
39. The unit cell parameters (triclinic, $P\bar{1}$) are as follows : a = 4.944(2) Å, b = 9.142(3) Å, c = 15.051(5) Å, α = 87.923(6)°, β = 84.590(6)°, γ = 78.759(7)°, V = 664.1(4) Å^3, Z = 1.

40. We thank N. S. Sampson and H. Tang for their help in measuring the electronic absorption spectrum of PIDA. We are grateful to NSF (grants CHE-9984937, CHE-0446749, and CHE-0453334) for financial support of this research. Crystallographic details for the **1•7** and **2•6** co-crystals are available free of charge from the Cambridge Crystallographic Data Centre under deposition numbers CCDC 294370 and CCDC 294371, respectively.

Supporting Online Material

www.sciencemag.org/cgi/content/full/312/5776/1030/DC1
Materials and Methods
Figs. S1 to S3
Tables S1 and S2

5 January 2006; accepted 17 March 2006
10.1126/science.1124621

Fast Mass Transport Through Sub–2-Nanometer Carbon Nanotubes

Jason K. Holt,[1]* Hyung Gyu Park,[1,2]* Yinmin Wang,[1] Michael Stadermann,[1] Alexander B. Artyukhin,[1] Costas P. Grigoropoulos,[2] Aleksandr Noy,[1] Olgica Bakajin[1]†

We report gas and water flow measurements through microfabricated membranes in which aligned carbon nanotubes with diameters of less than 2 nanometers serve as pores. The measured gas flow exceeds predictions of the Knudsen diffusion model by more than an order of magnitude. The measured water flow exceeds values calculated from continuum hydrodynamics models by more than three orders of magnitude and is comparable to flow rates extrapolated from molecular dynamics simulations. The gas and water permeabilities of these nanotube-based membranes are several orders of magnitude higher than those of commercial polycarbonate membranes, despite having pore sizes an order of magnitude smaller. These membranes enable fundamental studies of mass transport in confined environments, as well as more energy-efficient nanoscale filtration.

Carbon nanotubes, with diameters in the nanometer range and atomically smooth surfaces, offer a unique system for studying molecular transport and nanofluidics. Although the idea that water can occupy such confined hydrophobic channels is somewhat counterintuitive, experimental evidence has confirmed that water can indeed occupy these channels (*1*, *2*). Water transport through molecular-scale hydrophobic channels is also important because of the similarity of this system to transmembrane protein pores such as aquaporins (*3*). In recent years, numerous simulations (*4*, *5*) of water transport through single-walled carbon nanotubes (SWNTs) have suggested not only that water occupies these channels, but also that fast molecular transport takes place, far in excess of what continuum hydrodynamic theories would predict if applied on this length scale. Molecular dynamics (MD) simulations attribute this enhancement to the atomic smoothness of the nanotube surface and to molecular ordering phenomena that may occur on confined length scales in the 1- to 2-nm range (*4*, *5*). For similar reasons, simulations of gas transport through SWNTs (*6*) predict flux enhancements of several orders of magnitude relative to other similarly sized nanoporous materials. Membrane-based gas separations, such as those using zeolites (*7*), provide precise separation and size exclusion, although often at the expense of throughput or flux. It may be possible to use SWNTs to create a membrane that offers both high selectivity and high flux.

To investigate molecular transport on this length scale, we need to fabricate a carbon nanotube membrane that has a pore size of 1 to 2 nm. Researchers have recently fabricated multiwalled carbon nanotube (MWNT) membranes with larger pore diameters (6 to 7 nm) by encapsulation of vertically aligned arrays of MWNTs (*8*, *9*) and by templated growth within nanochannel alumina (*10*). Enhanced water transport through these larger MWNTs has recently been reported (*11*). Quantifying transport through an individual tube in a MWNT membrane is difficult, however, because MWNTs are prone to blockages, in particular by "bamboo" structures and catalyst particles that can migrate to and obstruct the nanotube interior (*9*, *12*, *13*). The consequence of such blockages is a marked reduction of the active membrane pore density. In contrast, there are few, if any, reports of "bamboo" structure formation or catalyst migration for SWNTs or double-walled carbon nanotubes (DWNTs). However, it is difficult to produce vertically aligned carbon nanotubes of this size (*14*, *15*). The major challenges also lie in finding a conformal deposition process to fill the gaps in this nanotube array, as well as in designing a selective etching process to open up the nanotube channels without producing voids in the membrane.

Table 1. Size exclusion tests on DWNT and MWNT membranes and molecular fluxes (per unit membrane area) of analytes. Values denoted by "<" were derived from the limits of detection for our concentration measurements when we did not observe any Au particles in the permeate solution. Differences of three to four orders of magnitude between this limiting value and the flux of the next smallest species indicate that the given analyte did not pass through the membrane.

Analyte	Analyte size (nm)	DWNT membrane flux (molecules cm^{-2} s^{-1})	MWNT membrane flux (molecules cm^{-2} s^{-1})
$Ru^{2+}(bipyr)_3$	1.3	5×10^{13}	5×10^{13}
Colloidal Au 1	2 ± 0.4	$<2 \times 10^{9}$	1×10^{11}
Colloidal Au 2	5 ± 0.75	$<3 \times 10^{8}$	3×10^{10}
Colloidal Au 3	10 ± 1	Not tested	$<4 \times 10^{7}$

[1]Chemistry and Materials Science Directorate, Lawrence Livermore National Laboratory, Livermore, CA 94550, USA. [2]Department of Mechanical Engineering, University of California, Berkeley, CA 94720, USA.

*These authors contributed equally to this work.
†To whom correspondence should be addressed. E-mail: bakajin1@llnl.gov

We have developed a microelectromechanical systems (MEMS)–compatible fabrication process (Fig. 1A) for sub–2-nm nanotube pore membranes. The process uses catalytic chemical vapor deposition to grow a dense, vertically aligned array of DWNTs on the surface of a silicon chip (Fig. 1B), followed by conformal encapsulation of the nanotubes by a hard, low-pressure chemical vapor–deposited silicon nitride (Si_3N_4) matrix (Fig. 1C). Scanning electron microscopy (SEM) images show that our process produces gap-free membranes over the length scale of the whole chip. The excess silicon nitride is removed from both sides of the membrane by ion milling, and the ends of the nanotubes are opened up with reactive ion etching. The membranes remain impermeable to both liquids and gases until the very last etching step; this is further evidence that our fabrication process produces crack-free and void-free membranes. Transmission electron microscopy (TEM) plan-view images (Fig. 2, C to E) of a slice of the membrane also demonstrate that the silicon nitride coats the DWNTs conformally and does not leave any gaps between the outer surface of the nanotube and the silicon nitride. We also used the same nitride-encapsulation method to produce MWNT membranes (*16*).

To characterize the membrane pore size, we performed size exclusion measurements (Table 1) (*16*) and compared these results with electron microscopy (EM) data. DWNT membranes passed species with sizes up to 1.3 nm yet blocked 2-nm gold particles, which suggests that these membranes have pore sizes between 1.3 and 2 nm. Comparison of the water flow rates before and during filtration, coupled with the upper-limit estimate of the flux of 2-nm gold particles, suggests that less than 0.1% of the flux through the membrane can be attributed to pores larger than 2 nm (*16*). These size exclusion measurements are further supported by the evidence obtained through EM. The distribution of DWNTs, as measured by TEM, revealed an inner diameter average of 1.6 nm (Fig. 2B). TEM images (Fig. 2C) of the membrane also revealed that the only holes that span the thickness of the membrane are of a size that is consistent with the inner diameter distribution of as-grown DWNTs. A MWNT membrane, used as a reference, transported colloidal gold particles with diameters of 2 and 5 nm but excluded the 10-nm colloidal gold particles, in agreement with MWNT diameters of 6.5 ± 0.5 nm estimated by TEM. This result also suggests that pore clogging by particles smaller than the average pore size is unlikely for the solution concentrations used in these experiments. We conclude that the transport in our samples occurs exclusively through the inner pores of the carbon nanotubes spanning the membrane.

The absolute gas flux through our membranes exceeded the flux predicted by the Knudsen diffusion model. As the dimensions

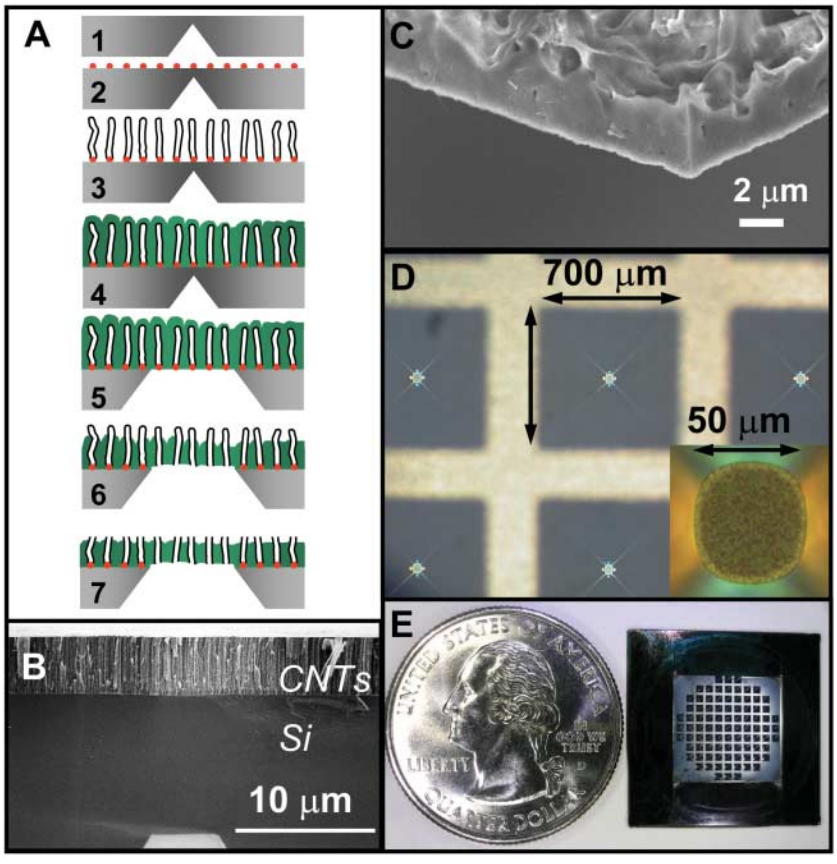

Fig. 1. (**A**) Schematic of the fabrication process. Step 1: microscale pit formation (by KOH etching). Step 2: catalyst deposition/annealing. Step 3: nanotube growth. Step 4: gap filling with low-pressure chemical vapor–deposited Si_3N_4. Step 5: membrane area definition (by XeF_2 isotropic Si etching). Step 6: silicon nitride etch to expose nanotubes and remove catalyst nanoparticles (by Ar ion milling); the membrane is still impermeable at this step. Step 7: nanotube uncapping (reactive ion etching); the membrane begins to exhibit gas permeability at this step. (**B**) SEM cross section of the as-grown DWNTs (CNTs). (**C**) SEM cross section of the membrane, illustrating the excellent gap filling by silicon nitride. (**D**) Photograph of the open membrane areas; inset shows a close-up of one membrane. (**E**) Photograph of the membrane chip that contains 89 open windows; each window is 50 μm in diameter.

Table 2. Comparisons of experimental air flow rates observed for several DWNT membranes with Knudsen model predictions, and of experimental water flow rates with continuum flow model predictions. The differences among the three DWNT membranes are most likely the result of different numbers of pores opened in the fabrication process. Values for a polycarbonate membrane are provided as a reference. Pore diameters were determined from size exclusion measurements, TEM measurements, and (for polycarbonate) manufacturer's specifications. Pore density values are upper limits, as determined from TEM measurements and (for polycarbonate) manufacturer's specifications.

Membrane	Pore diameter (nm)	Pore density (cm^{-2})	Thickness (μm)	Enhancement over Knudsen model* (minimum)	Enhancement over no-slip, hydrodynamic flow† (minimum)	Calculated minimum slip length‡ (nm)
DWNT 1	1.3 to 2.0	$\leq 0.25 \times 10^{12}$	2.0	40 to 120	1500 to 8400	380 to 1400
DWNT 2	1.3 to 2.0	$\leq 0.25 \times 10^{12}$	3.0	20 to 80	680 to 3800	170 to 600
DWNT 3	1.3 to 2.0	$\leq 0.25 \times 10^{12}$	2.8	16 to 60	560 to 3100	140 to 500
Polycarbonate	15	6×10^{8}	6.0	2.1	3.7	5.1

*From (*18*). †From (*26*). ‡From (*29*).

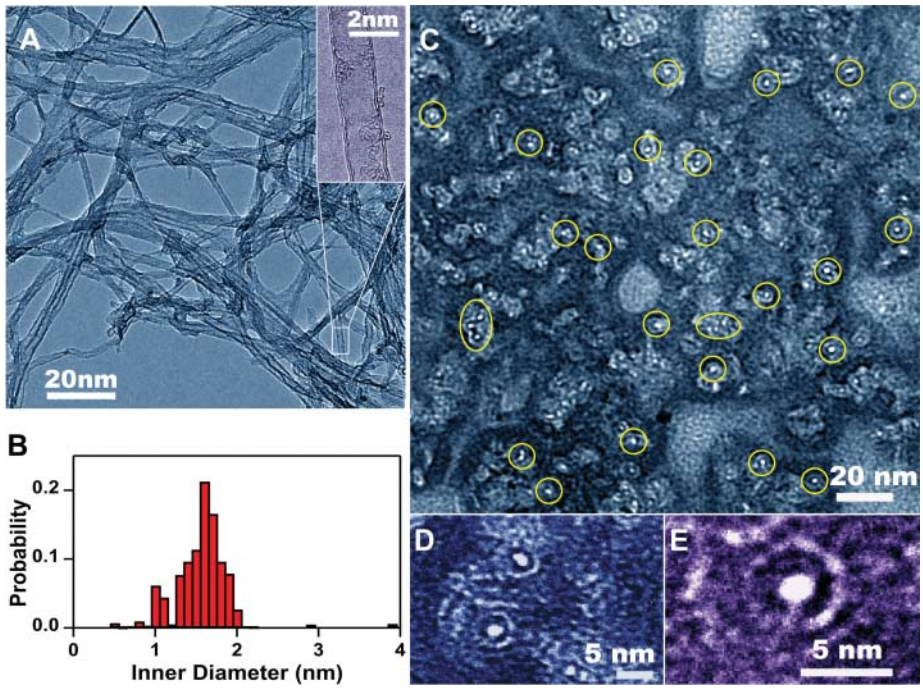

Fig. 2. (**A**) TEM images of as-grown nanotubes, prepared by removing them from the silicon substrate and dispersing them in dimethylformamide. The majority of the carbon nanotubes are double-walled, as identified in the high-resolution inset. (**B**) Pore size distribution, derived from TEM measurements of the inner diameter of 391 individual carbon nanotubes, reveals an average pore size of 1.6 nm. The average outer diameter of these DWNTs is estimated to be 2.3 nm. (**C** to **E**) Plan-view TEM images of carbon nanotube membrane taken with the beam parallel to the nanotube axis. In (C), the nanotube membrane shows continuous nitride coating on the scales examined in this image (~0.2 μm by 0.2 μm). No microcracks or microvoids can be seen. The bright white spots (circled in yellow) are carbon nanotube pores, which can be identified by the surrounding ring-shaped coating of silicon nitride. For clarity, not all visible nanotubes were circled. The density of carbon nanotubes is measured to be $\sim 2.5 \times 10^{11}$ cm^{-2} from several similar TEM images. In (D) and (E), high-resolution TEM images of selected areas from (C) show conformal coating of silicon nitride. The bright white spots in the images have the same inner diameter as the carbon nanotubes.

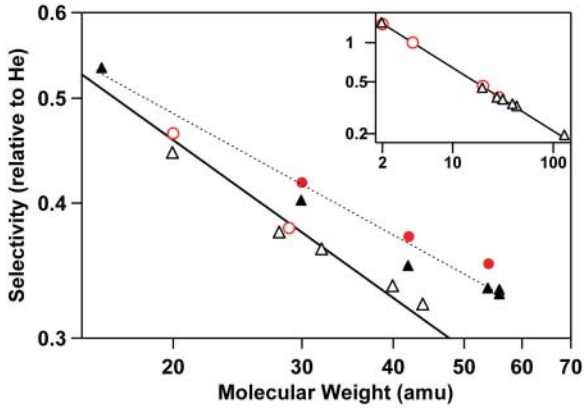

Fig. 3. Gas selectivity (defined as permeability relative to He) data for sub–2-nm DWNT (triangles) and MWNT (circles) membranes. Open symbols denote nonhydrocarbon gases (H_2, He, Ne, N_2, O_2, Ar, CO_2, Xe); solid symbols denote hydrocarbon gases (CH_4, C_2H_6, C_3H_6, C_4H_6, C_4H_8). The solid line is a power-law fit of the nonhydrocarbon gas selectivity data, showing a scaling predicted by the Knudsen diffusion model (exponent of –0.49 ± 0.01). The dashed line is a power-law fit of the hydrocarbon gas data, showing a deviation from the Knudsen model (exponent of –0.37 ± 0.02). The inset shows the full mass range of the nonhydrocarbon gas data, again illustrating agreement with the Knudsen model scaling.

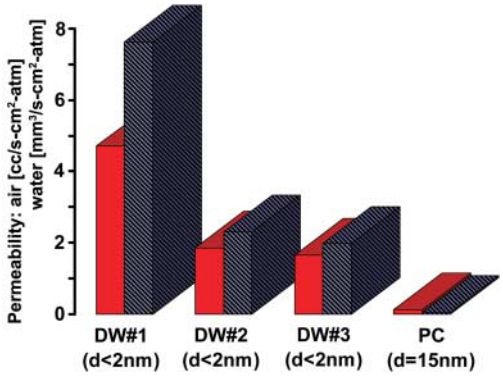

Fig. 4. Air (red) and water (blue) permeability as measured for three DWNT membranes (DW#1, 2, and 3) and a polycarbonate membrane (PC). Despite considerably smaller pore sizes, the permeabilities for all DWNT membranes greatly exceed those of the polycarbonate membrane.

of the pore shrink, the mean free path (λ) becomes larger than the channel dimensions (*d*) and the transport enters the molecular flow regime. In such situations, where particle-surface collisions dominate over particle-particle collisions, the Knudsen diffusion model (*17*) is frequently applied. Indeed, our pore geometries are characterized by Knudsen numbers (λ/*d*) of 10 to 70, which places them well into the free molecular transport regime. However, the flux measured through our membranes exceeded the flux predicted by the Knudsen model (*18*) by at least one to two orders of magnitude (Table 2). By comparison, a polycarbonate membrane (Nucleopore, Osmonics Inc.) revealed just a slight enhancement in flux. The single largest uncertainty in quantifying the flux through our membrane pores lies in determination of the active pore density (i.e., those nanotubes that are open and spanning the membrane). A pore density estimate of 2.5×10^{11} cm^{-2} was derived from the plan-view TEM images of the DWNT membrane (Fig. 2, C to E), and the enhancement factors that we report represent lower boundary estimates (*19*). The observed flow enhancement is most likely caused by the intrinsic smoothness of the nanotube surface, as predicted by MD simulations of gas flow through SWNTs (*6*, *20*–*22*). In atomically smooth pores, the nature of gas-wall collisions can change from purely diffuse (as in the Knudsen model) to a combination of specular and diffuse collisions (*23*), thus leading to observed faster transport.

We found that single-component selectivity for most of the gases exhibited the expected inverse-square-root scaling of molecular mass (Fig. 3, inset) with the exception of hydrocarbons, whose selectivities were higher. This result is not surprising for a molecular diffusion process because it reflects the mass dependence of molecular velocity (note that the nature of wall collisions would not affect the mass scaling). Of all the measured gases, only the hydrocarbons deviated from this pattern, exhibiting a higher selectivity (Fig. 3) in both DWNT

and MWNT membranes. Interestingly, a reference polycarbonate membrane with a pore size of 15 nm did not show this deviation. We attribute the deviation to the preferential interaction of hydrocarbons with the carbon nanotube sidewalls. The hydrocarbon transport enhancement most likely results from surface diffusion or possibly a solubility/diffusion mechanism (*24*). Pulse mass analysis of various organic compounds has shown strong adsorption of hydrocarbon molecules (e.g., hexane) on SWNTs relative to more polar molecules (e.g., ethanol) (*25*). It is noteworthy that the hydrocarbon selectivity we observe in these single-component experiments may be more pronounced for practical gas separation problems where mixtures are involved (*20*).

Our membranes also transported water across the carbon nanotube channels at rates that cannot be accounted for by continuum flow models. The measured water flow rates reveal a flow enhancement (Table 2) that is more than three orders of magnitude faster than the no-slip, hydrodynamic flow as calculated from the Hagen-Poiseuille equation (*26*). Breakdown of this continuum model is not surprising for channels 1 to 2 nm in size. If we take the formalism used for gases and define a mean free path in liquids as the molecular diameter (e.g., ~0.3 nm for H_2O), the Knudsen number for a 1- to 2-nm pore is 0.15 to 0.3. These values lie on the border between "slip flow" and "transitional flow." In this size regime, where the pore is only ~7 water molecules in diameter, continuum theory concepts such as a velocity profile may be difficult to define. For this reason, MD simulations are often used for the prediction of water flows through carbon nanotube pores with diameters on the order of 1 nm (*4*, *5*). However, the computational expense of MD simulations, as well as observations of a finite fluid "slipping velocity" at hydrophobic interfaces (*27*), have motivated attempts to use meso- and macroscopic flow models to simulate flow through SWNTs (*28*). These simulations calculated a corresponding "slip length" that describes the noncontinuum behavior of a liquid near the pore walls. If we apply a similar formalism for the flow through our sub–2-nm nanotube membranes, we calculate (*29*) slip lengths as large as 1400 nm (Table 2). These values are almost three orders of magnitude larger than the pore size and are on the order of the overall size of the system (pore length). In contrast, the polycarbonate membrane with a pore size of 15 nm reveals a much smaller slip length of just 5 nm. This comparison suggests that slip-flow formalism may not be applicable to water flow through sub–2-nm carbon nanotubes, possibly because of length scale confinement (*30*) or partial wetting of the carbon nanotube surface (*31*).

Our observed water flux compares well with that predicted by the MD simulations (*5*). The simulations predict a flux of 12 water molecules through 1 nm^2 of the nanotube cross-sectional area in 1 ns; our measured flux, extrapolated to the simulation pressure drop, corresponds to 10 to 40 water molecules nm^{-2} ns^{-1} (*32*). The MD simulations attributed the observed high water flow rates to the formation of water "wires" in the confined space inside the nanotube. The strong dependence of the structure of the water in the nanotube on diameter (*33*) indicates that small differences in nanotube diameter can have large effects on transport. Therefore, it is unclear whether the mechanism proposed by MD is responsible for the high water flow rates observed with the larger nanotubes used in our experiments, or whether the flow enhancement can be attributed simply to the presence of a nearly frictionless surface.

Membrane permeability provides a figure of merit for membrane performance for practical applications. Despite having an order of magnitude smaller pore size, the enhanced flow rate per pore and the higher pore density render the sub–2-nm membranes superior to conventional polycarbonate membranes in both air and water permeability (*34*) (Fig. 4).

References and Notes

1. A. I. Kolesnikov *et al.*, *Phys. Rev. Lett.* **93**, 035503 (2004).
2. N. Naguib *et al.*, *Nano Lett.* **4**, 2237 (2004).
3. P. Agre *et al.*, in *Aquaporins*, S. Hohmann, S. Nielsen, P. Agre, Eds., vol. 51 of *Current Topics in Membranes* (Academic Press, San Diego, CA, 2001), pp. 1–38.
4. G. Hummer, J. C. Rasaiah, J. P. Noworyta, *Nature* **414**, 188 (2001).
5. A. Kalra, S. Garde, G. Hummer, *Proc. Natl. Acad. Sci. U.S.A.* **100**, 10175 (2003).
6. A. I. Skoulidas, D. M. Ackerman, J. K. Johnson, D. S. Sholl, *Phys. Rev. Lett.* **89**, 185901 (2002).
7. Z. Lai *et al.*, *Science* **300**, 456 (2003).
8. B. J. Hinds *et al.*, *Science* **303**, 62 (2004); published online 26 November 2003 (10.1126/science.1092048).
9. J. K. Holt, A. Noy, T. Huser, D. Eaglesham, O. Bakajin, *Nano Lett.* **4**, 2245 (2004).
10. J. Li, C. Papadopoulos, J. M. Xu, M. Moskovits, *Appl. Phys. Lett.* **75**, 367 (1999).
11. M. Majumder, N. Chopra, R. Andrews, B. J. Hinds, *Nature* **438**, 44 (2005).
12. Y. Y. Wang, S. Gupta, R. J. Nemanich, Z. J. Liu, L. C. Qin, *J. Appl. Phys.* **98**, 014312 (2005).
13. H. Cui, O. Zhou, B. R. Stoner, *J. Appl. Phys.* **88**, 6072 (2000).
14. S. Maruyama, E. Einarsson, Y. Murakami, T. Edamura, *Chem. Phys. Lett.* **403**, 320 (2005).
15. K. Hata *et al.*, *Science* **306**, 1362 (2004).
16. See supporting material on *Science* Online.
17. A. F. Mills, *Mass Transfer* (Prentice-Hall, Upper Saddle River, NJ, 2001), pp. 68–69.
18. For gas flow in the Knudsen regime, the overall membrane flow rate can be determined from

$$Q_{gas} = \frac{2}{3}\sqrt{\frac{8\pi}{MRT}}(d/2)^3 V_m \frac{\Delta p}{L}\sigma A$$

where M is molecular weight, R is the universal gas constant, T is absolute temperature, d is pore diameter, V_m is the molar volume, Δp is the pressure drop, L is the thickness of the membrane, σ is the areal pore density, and $A = 89 \cdot \pi(25\ \mu m)^2 = 175{,}000\ \mu m^2$ is the total area of the membrane.
19. This density is only a factor of 4 smaller than the catalyst density on the substrate (~10^{12} cm^{-2}), also determined by TEM. This areal density is comparable to the measured areal density of SWNTs/DWNTs produced using a catalyst recipe similar to the one we used (*12*). The estimate from the TEM images still represents the upper bound for the density because it assumes that every DWNT that spans the section imaged in the TEM (thickness 50 nm) also spans the entire membrane thickness.
20. H. B. Chen, D. S. Sholl, *J. Membr. Sci.* **269**, 152 (2006).
21. D. M. Ackerman, A. I. Skoulidas, D. S. Sholl, J. K. Johnson, *Mol. Sim.* **29**, 677 (2003).
22. H. B. Chen, J. K. Johnson, D. S. Sholl, *J. Phys. Chem. B* **110**, 1971 (2006).
23. S. K. Bhatia, H. B. Chen, D. S. Sholl, *Mol. Sim.* **31**, 643 (2005).
24. C. Leger, H. D. Lira, R. Paterson, *J. Membr. Sci.* **120**, 187 (1996).
25. E. W. Bittner, M. R. Smith, B. C. Bockrath, *Carbon* **41**, 1231 (2003).
26. The Hagen-Poiseuille equation is

$$Q_{HP} = \frac{\pi(d/2)^4}{8\mu}\frac{\Delta p}{L}$$

where Q_{HP} is the volumetric flow rate, Δp is the pressure drop, d is the pore diameter, μ is the water viscosity, and L is the membrane thickness.
27. J. Baudry, E. Charlaix, A. Tonck, D. Mazuyer, *Langmuir* **17**, 5232 (2001).
28. E. M. Kotsalis, J. H. Walther, P. Koumoutsakos, *Int. J. Multiphase Flow* **30**, 995 (2004).
29. With the inclusion of a slip-flow correction, the Hagen-Poiseuille equation becomes

$$Q_{SLIP} = \frac{\pi\left[(d/2)^4 + 4(d/2)^3 L_s\right]}{8\mu}\frac{\Delta p}{L}$$

where L_s is defined as the slip length,

$$L_s = \frac{U_{wall}}{dU/dr}$$

where U_{wall} is the axial velocity at the wall, and dU/dr is the radial velocity gradient at the wall (or shear rate).
30. C. Cottin-Bizonne *et al.*, *Eur. Phys. J. E* **9**, 47 (2002).
31. V. S. J. Craig, C. Neto, D. R. M. Williams, *Phys. Rev. Lett.* **87**, 054504 (2001).
32. The simulation considered water transport across the carbon nanotubes driven by an osmotic pressure of about 100 atm. Our experiments used pressure drops of 1 atm. We have also observed linear dependence between the applied pressure drop and the flow rate across the membranes. As an approximation, we therefore used a linear extrapolation to compare our measured flows to the simulation results. We note two key differences between our experiments and the simulations: (i) The simulations used nanotubes 0.8 nm in diameter, whereas our samples were 1.6 nm in diameter on average; and (ii) the pressure drops were ~100 atm in the simulations versus 1 atm in our experiments, and it is unclear whether our linear extrapolation in flow rate versus pressure drop is valid over this range.
33. K. Koga, G. T. Gao, H. Tanaka, X. C. Zeng, *Nature* **412**, 802 (2001).
34. Permeability is defined as the volumetric flux, normalized by the pressure drop.

35. We thank J. Muyco for help with Raman spectroscopy, R. Friddle for assistance with atomic force microscopy measurements, W. J. Moberlychan for his assistance on FIB and TEM experiments, and D. Eaglesham for early contributions to the project and lively discussions. This work was performed under the auspices of the U.S. Department of Energy by University of California Lawrence Livermore National Laboratory under contract W-7405-Eng-48 with funding from the Laboratory Directed Research and Development Program. H.G.P. and A.B.A. were supported by a Student Employee Graduate Research Fellowship.

Supporting Online Material

www.sciencemag.org/cgi/content/full/312/5776/1034/DC1
Materials and Methods
Fig. S1

15 February 2006; accepted 15 March 2006
10.1126/science.1126298